npj | precision oncology

Article

Published in partnership with The Hormel Institute, University of Minnesota

https://doi.org/10.1038/s41698-025-00967-w

Multi-omics analyses reveal interactions between GREM1+ fibroblasts and SPP1+ macrophages in gastric cancer

Lupeng Qiu[1,2,5], Xiao Zhao[3,5], Sheng Yao[4], Yang Fei[4], Yixin Gong[2], Zishan Zhou[2], Shunchang Jiao[3] ✉ & Jianming Xu[1,3] ✉

Gastric cancer (GC) is among the most lethal human malignancies with limited treatment options. Cell-cell interactions within the tumor microenvironment (TME) can promote tumor growth, yet their therapeutic value has not been fully explored. Here, bulk RNA-seq, single-cell RNA sequencing (scRNA-seq), and spatial transcriptomics (ST) were integrated to analyze the heterogeneity of GC microenvironment. Tumor-specific GREM1+ fibroblasts and SPP1+ macrophages were significantly enriched in GC tissues and were involved in immunosuppression, inflammation regulation, and tumor progression. We then indicated that GREM1+ fibroblasts and SPP1+ macrophages were positively correlated in 12 independent GC datasets and validated their close localization by multiplex immunohistochemistry staining and spatial transcriptomics. Patients with both high GREM1+ fibroblasts and SPP1+ macrophages exhibited significantly shorter OS and showed enrichment of tumor-associated pathways. Our results demonstrated the complex interactions between GREM1+ fibroblasts and SPP1+ macrophages, which may serve as a potential therapeutic target for future treatment of GC.

Gastric cancer (GC) is one of the most common malignancies worldwide and an important cause of cancer-related death[1,2]. At present, surgical resection is considered the only potentially curative treatment for GC, which has greatly improved the prognosis of these patients[3]. However, the recurrence rate is still high in patients undergoing surgical resection, while the prognosis is worse in unresectable patients. Chemotherapy, targeted therapy, and immunotherapy are the main treatment methods for advanced gastric cancer, but they are faced with the problems of recurrence, metastasis, and drug resistance[4–6]. Researchers have gradually changed the research strategy from tumor cells to a biological model with TME, which also provides a new opportunity for the treatment of GC.

The tumor microenvironment (TME) is mainly composed of cell components such as lymphocytes, myeloid cells, and fibroblasts, and non-cellular components such as blood vessels, extracellular matrix, and cytokines[7]. In recent years, more and more studies have found that TME plays an important role in regulating immune function, angiogenesis, and drug efficacy[8]. Cancer-associated fibroblast (CAF) is a common type of stromal cell in TME, which can affect tumor progression and drug resistance by regulating connective tissue proliferation, angiogenesis, immune regulation, and tumor metabolism[9,10]. Tumor-associated macrophage (TAM) is also an important class of immune cells, which can have important effects on the occurrence and progression of tumor[11]. TAM can be further divided into M1 type and M2 type, wherein M1 macrophages have anti-tumor and pro-inflammatory functions, while M2 macrophages have anti-inflammatory and pro-tumor functions[12,13]. With the rapid development of single-cell RNA sequencing (scRNA-seq) and spatial transcriptomics (ST), we can more accurately annotate the function and heterogeneity of cell subsets, providing a direction for in-depth exploration of TME.

It has been reported that both CAFs and TAMs are essential components of the TME and play critical roles in the regulation of tumor progression[14]. TAMs are the most abundant immune cells in areas of CAFs, indicating a close interaction between these two cell types[15]. CAFs can secrete a variety of regulatory molecules to promote monocyte recruitment and differentiation into M2 macrophages, and in turn, M2 macrophages can also regulate the activation and progression of CAFs[16]. Comito et al. found that M2 macrophages can secrete IL-6 and SDF-1, stimulate CAFs activation, and promote epithelial-mesenchymal transformation[17]. Zhang et al. revealed that macrophages can promote mesenchymal cells to acquire

[1]Department of Medical Oncology, The First Medical Centre, Chinese PLA General Hospital, Beijing, China. [2]Research and Development Department, Beijing DCTY Biotech Co., Ltd., Beijing, China. [3]Department of Medical Oncology, The Fifth Medical Centre, Chinese PLA General Hospital, Beijing, China. [4]Department of General Surgery, The First Medical Centre, Chinese PLA General Hospital, Beijing, China. [5]These authors contributed equally: Lupeng Qiu, Xiao Zhao. ✉e-mail: scjiao301@126.com; jmxu2003@163.com

CAF-like phenotypes and properties, reshape TME, and promote malignant transformation of epithelial cells[18]. However, due to the complexity of TME and the limitations of research methods, the detailed molecular mechanisms of this interaction remain elusive. The rise of scRNA-seq technology, advances in bioinformatics, and the integration of morphology, spatial localization, and transcriptome features have opened a new window to reveal the cellular communication and conduction networks during tumor development.

Here, scRNA-seq combined with ST was used to analyze the heterogeneity of GC microenvironment. Our study led to the identification of seven subtypes of fibroblasts and four subtypes of macrophages. Among these subtypes, we specifically focused on the GREM1+ CAFs and SPP1+ TAMs. Recent studies have shown that GREM1 is a biomarker of myofibroblasts, and it plays an important role in promoting tumor progression through the activation of fibrosis, angiogenesis, and epithelial-mesenchymal transition[19]. Similarly, SPP1+ TAM is a type of M2 macrophage with profibrotic characteristics[20]. Through in-depth analyses, we found that GREM1+ CAFs and SPP1+ TAMs localized in neighboring areas. Intercellular communication analysis demonstrated that there were close communication relationships between these two cell types. Furthermore, high infiltration of GREM1+ CAFs and SPP1+ TAMs was correlated with worse prognosis. Together, our study unravels the complex interactions between GREM1+ CAFs and SPP1+ TAMs, which may serve as a potential therapeutic target for future GC treatment.

Results

A single-cell transcriptomics atlas of heterogeneous tumor microenvironment in GC

In this study, the training cohort consisted of four published gastric cancer scRNA-seq datasets, including 48 gastric cancer tissues and 24 adjacent normal tissues. After quality control filtering, a total of 151, 869 cell transcriptomes were retained for subsequent analysis, with batch effects across different samples being removed by "harmony" package. The cells were classified into 9 major cell types based on their representative classification markers: 66, 556 T/NK cells marked by CD3E and NKG7, 19, 923 plasma cells marked by IGLL5 and MZB1, 14, 028 fibroblasts marked by COL1A1 and DCN, 13, 699 myeloid cells marked by S100A9 and CD14, 12, 130 epithelial cells marked by EPCAM and KRT8, 11, 431 B cells marked by MS4A1 and CD79A, 7, 906 endothelial cells marked by PLVAP and VWF, 3, 401 mast cells marked by KIT and MS4A2, and 2, 795 proliferative cells marked by MKI67 and TOP2A (Figs. 1A, B and S1). Although all 9 major cell types were presented in both tumor and adjacent normal tissues, the percentage of each cell type was different. Myeloid cells, mast cells, and proliferative cells had higher infiltration levels in tumor tissues than in adjacent normal tissues (Fig. 1C–E).

Tumor-related GREM1+ fibroblasts are associated with GC progression

Cancer-associated fibroblasts are recognized as key components of the tumor microenvironment and are known to promote tumorigenesis and metastasis. However, the study of CAFs was still very difficult, largely due to their heterogenous nature. In this study, fibroblasts were divided into 7 subclusters after dimension reduction clustering, named c1-POSTN ($n = 5854$), c2-RGS5 ($n = 2592$), c3-HILPDA ($n = 2203$), c4-C7 ($n = 1487$), c5-GREM1 ($n = 779$), c6-CALB2 ($n = 560$), and c7-IGF1 ($n = 553$), respectively (Fig. 2A, B). GREM1+ fibroblasts were significantly enriched in tumor tissues, while CALB2+ fibroblasts were enriched in adjacent normal tissues (Fig. 2C). Fibroblasts exhibited a high degree of functional heterogeneity. GREM1+ fibroblasts had the highest scores for EMT, angiogenesis and M2 macrophage polarization, while C7+ fibroblasts had the highest scores for complement activation (Fig. S2). GSVA of the hallmark pathways revealed that GREM1+ fibroblasts had a higher enrichment score for notch signaling, epithelial mesenchymal transition and angiogenesis, indicating that GREM1+ fibroblasts could promote GC progression (Fig. 2D). The pseudotime of the developmental trajectory showed that GREM1+ fibroblasts may have an impact at later stages (Fig. 2E, F). Subsequently, we analyzed the association between GREM1+ fibroblasts and clinical features in TCGA-STAD dataset using the ssGSEA algorithm. The results showed that GREM1+ fibroblasts were significantly enriched in GC tissues, and patients with high expression of GREM1+ fibroblasts were associated with poor TNM stage and survival (Fig. 2G–J).

Tumor-related SPP1+ macrophages are associated with GC progression

Myeloid cells are one of the most abundant stromal cells in the tumor microenvironment and play an important role in tumor initiation and progression. In this study, myeloid cells were divided into 9 subclusters after dimension reduction clustering, named c1-macro-SPP1 ($n = 3044$), c2-macro-C1QB ($n = 2774$), c3-macro-INHBA ($n = 1098$), c4-macro-CXCL9 ($n = 1074$), c5-mono-FCN1 ($n = 1561$), c6-mono-CCL20 ($n = 1458$), c7-dc-CD1C ($n = 791$), c8-dc-LAMP3 ($n = 668$) and c9-neu-FCGR3B ($n = 1231$), respectively (Fig. 3A, B). SPP1+ macrophages were significantly enriched in tumor tissues, and CD1C+ dendritic cells were enriched in adjacent normal tissues (Fig. 3C). CXCL9+ macrophages had the highest M1 macrophage polarization scores with high expression of CXCL9, CXCL10 and CD80, while SPP1+ macrophages had the highest M2 macrophage polarization scores, with high expression of FN1, CD14 and CD163 (Fig. S3). GSVA of the hallmark pathways revealed that SPP1+ macrophages had a higher enrichment score for angiogenesis, coagulation, hypoxia, and glycolysis, indicating that SPP1+ macrophages could promote GC progression (Fig. 3D). The pseudotime of the developmental trajectory showed that SPP1+ macrophages have an impact at later stages (Fig. 3E, F). We then analyzed the association between SPP1+ macrophages and clinical features in TCGA-STAD dataset. The results showed that SPP1+ macrophages were significantly enriched in GC tissues, and patients with high expression of SPP1+ macrophages were associated with poor TNM stage and survival (Fig. 3G–J).

Interactions between GREM1+ fibroblasts and SPP1+ macrophages

To further confirm these findings, we performed single-cell analysis in our own cohort. The results showed that both GREM1+ fibroblasts and SPP1+ macrophages were significantly enriched in GC tissues (Fig. S4). Recent studies have shown that fibroblasts and macrophages can influence each other to synergistically drive tumor progression. Given the above results, we used the ssGSEA algorithm to assess the interactions between GREM1+ fibroblasts and SPP1+ macrophages in 12 independent GC datasets. The results indicated that GREM1+ fibroblasts and SPP1+ macrophages were positively correlated across all examined datasets (Fig. 4A).

We further investigated whether GREM1+ fibroblasts and SPP1+ macrophages localize closely in GC tissues. Immunofluorescent labeling indicated close proximity between GREM1-positive and SPP1-positive cells, suggesting a potential crosstalk between these two cell types (Fig. 4B). Spatial transcriptomics can be used to reveal the location of different cell types and their interactions. Based on the unbiased clustering and spot features, we classified the spots into 10 clusters, plasma cells, immune cells, fibroblasts, epithelial cells, malignant epithelial cells, GREM1+ fibroblasts, SPP1+ macrophages, macrophages, B cells, and endothelial cells of patient #4 (Fig. 5A-C). We also classified the spots of patient #5 into 10 clusters, MT+ cells, fibroblasts, epithelial cells, malignant epithelial cells, plasma cells, GREM1+ fibroblasts, myofibroblasts, endothelial cells, SPP1+ macrophages, and B cells (Fig. 5D–F). Results presented above suggest that GREM1+ fibroblasts and SPP1+ macrophages localized in neighboring areas. Score spots in each cluster with GREM1+ fibroblasts or SPP1+ macrophage signatures from scRNA-seq data highlighted the spatial proximity of the two cell types (Fig. 5G–J).

High infiltration of GREM1+ fibroblasts and SPP1+ macrophages correlates with worse patient prognosis

To further uncover the clinical implication of such close correlation between these two cell types, we compared the OS of patients with different levels of

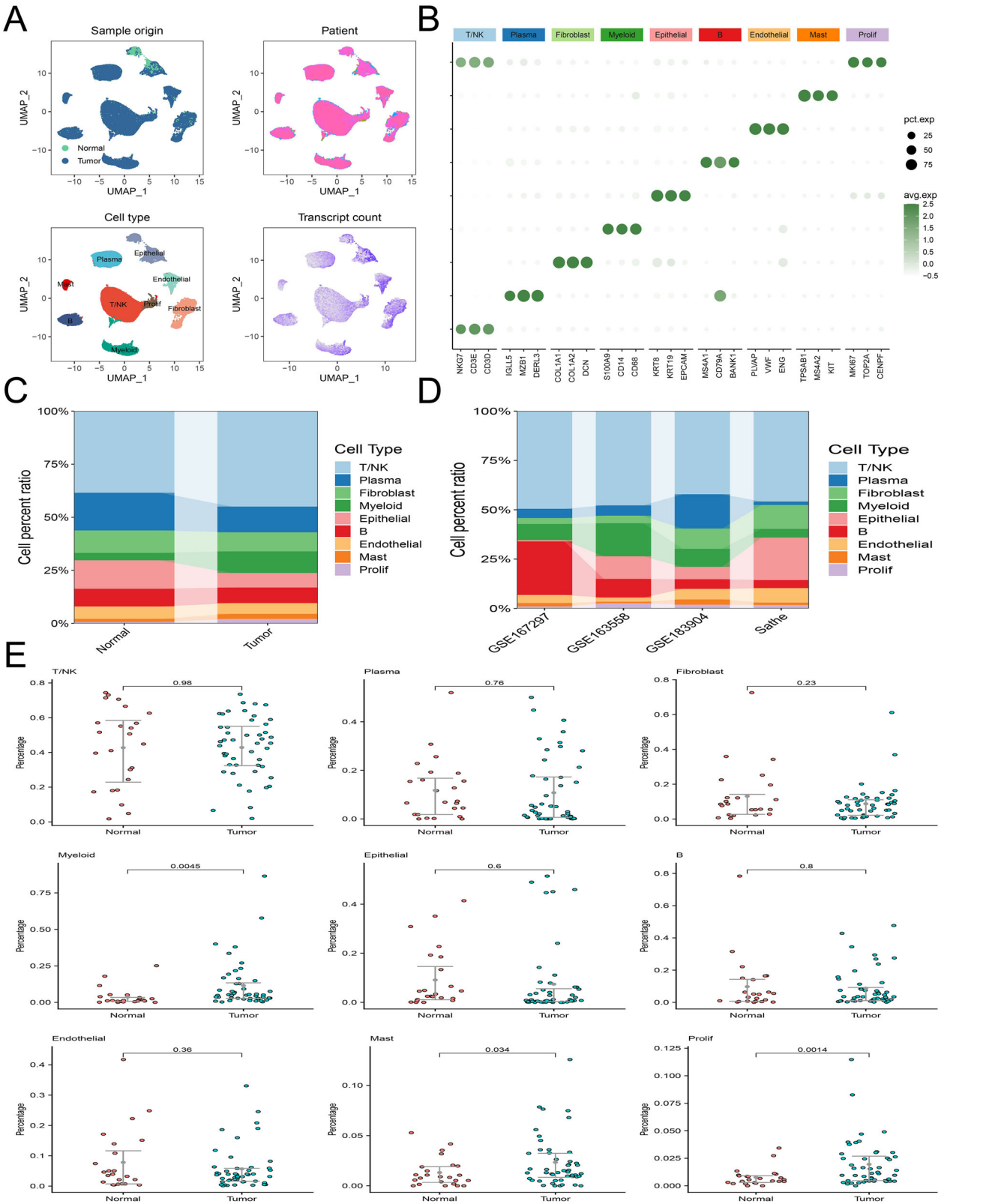

Fig. 1 | Single-cell transcriptomics atlas of heterogeneous tumor microenvironment in GC patients. A UMAP plots of clustered scRNA-seq data from combined samples. **B** Dot plots showing the top three differentially expressed genes of 9 major cell types. **C** Proportion of cell types in different tissues. **D** Proportion of cell types in different scRNA-seq datasets. **E** Proportion of cell types in each sample.

GREM1+ fibroblasts and SPP1+ macrophages. Patients with both high GREM1+ fibroblasts and SPP1+ macrophages exhibited significantly shorter OS compared with other groups, suggesting that these two cell types can synergistically promote GC progression (Fig. 6A, B). GO analysis showed significant enrichment of terms such as extracellular matrix structure, collagen containing extracellular matrix, and myeloid leukocyte migration in patients with GREM1+ fibroblast^{high}/SPP1+ macrophage^{high} (Fig. 6C). GSEA analysis indicated that genes upregulated in the high

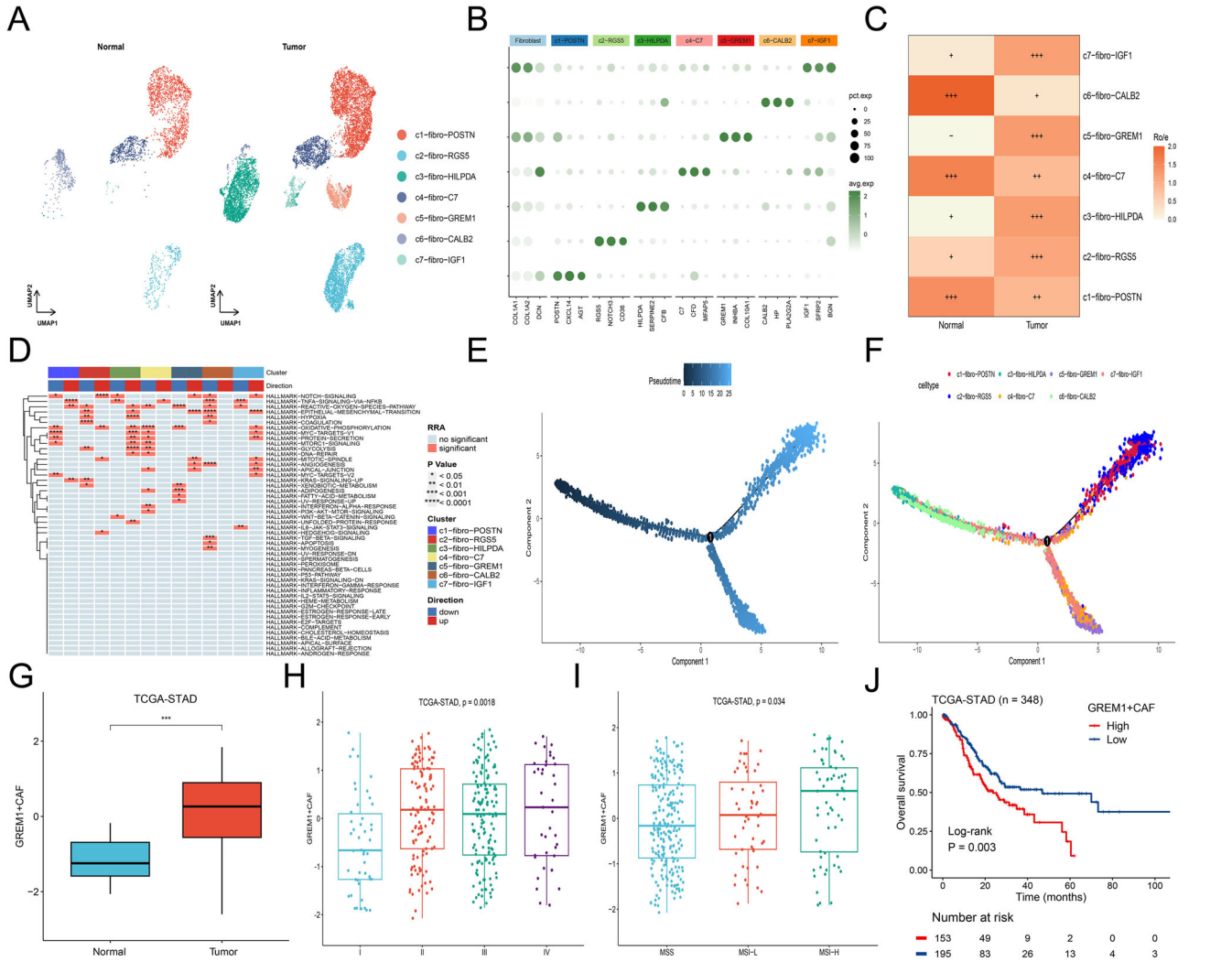

Fig. 2 | Characterization of fibroblasts in GC patients. A UMAP plot showing the composition of fibroblasts colored by cluster. **B** Dot plot showing the top three differentially expressed genes of 7 fibroblast clusters. **C** Tissue preference of each fibroblast cluster estimated by Ro/e score. +++, Ro/e > 1; ++, 0.8 < Ro/e ≤ 1; +, 0.2 ≤ Ro/e ≤ 0.8; ±, 0 < Ro/e < 0.2; −, Ro/e = 0. **D** GSVA plot showing the terms of the hallmark gene set enrichment pathway for each fibroblast cluster. **E** The pseudotime of the developmental trajectory inferred by Monocle 2. **F** Fibroblast transition along the pseudotime trajectory. **G** Quantification of GREM1+ fibroblast in TCGA-STAD dataset. **H** Association between GREM1+ fibroblast and TNM stage. **I** Association between GREM1+ fibroblast and microsatellite status. **J** K-M curves of OS in TCGA-STAD dataset grouped by GREM1+ fibroblast.

expression group showed enrichment of TGF-β, axon development, epithelial to mesenchymal transition, and antigen processing and presentation pathways (Fig. 6D).

GC is a heterogeneous cancer that can be subtyped based on molecular signatures. Therefore, knowledge of GC molecular subtypes might help to identify patients for the most appropriate treatment options. Based on the infiltration levels of GREM1+ fibroblasts and SPP1+ macrophages, patients were divided into three groups: low (GREM1+ fibroblast^{low}/SPP1+ macrophage^{low}), intermediate (GREM1+ fibroblast^{high}/SPP1+ macrophage^{low} or GREM1+ fibroblast^{low}/SPP1+ macrophage^{high}), and high (GREM1+ fibroblast^{high}/SPP1+ macrophage^{high}). In TCGA-STAD and GSE62254 datasets, the proportion of diffuse subtype in the high group was 36.5% and 56.3%, respectively, which were significantly higher than those in the low group (15.8% and 30.3%) (Fig. 7A–D). We then analyzed the infiltration levels of tumor infiltrating immune cells in different subtypes, and found that the percentage of patients in the high group was generally higher than that in the intermediate and low group (Fig. 7E). The ESTIMATE algorithm also showed that patients in the high group had the highest immune and stromal scores, while patients in the low group had the highest tumor purity (Fig. 7F). In the IMvigor210 cohort, Kaplan-Meier analysis indicated that patients in the high group had worse survival outcomes after receiving immunotherapy (Fig. 7G–J).

Cell-cell interactions of GREM1+ fibroblasts and SPP1+ macrophages revealed by scRNA-seq and spatial transcriptomics

In order to clarify the cell-cell interaction mechanisms between GREM1+ fibroblasts and SPP1+ macrophages, we built separate intercellular communication networks based on the scRNA-seq and spatial transcriptomics data. Results of spatial transcriptomics revealed that GREM1+ fibroblasts can directly contact with SPP1+ macrophages through COLLAGEN signaling pathway, while SPP1+ macrophages can also act on GREM1+ fibroblasts through SPP1 signaling pathway (Figs. 8A–D and S5). As demonstrated in Fig. 8E–L, SPP1-ITGAV/ITGB5 signal axis was distributed over neighboring sites. For single-cell analysis, we also found that there were close communication relationships between GREM1+ fibroblasts and SPP1+ macrophages (Fig. S6A–C). Similar to the results of spatial transcriptome analysis, the SPP1 and COLLAGEN signaling pathways were the main functional pathways between GREM1+ fibroblasts and SPP1+ macrophages (Fig. S6D–G).

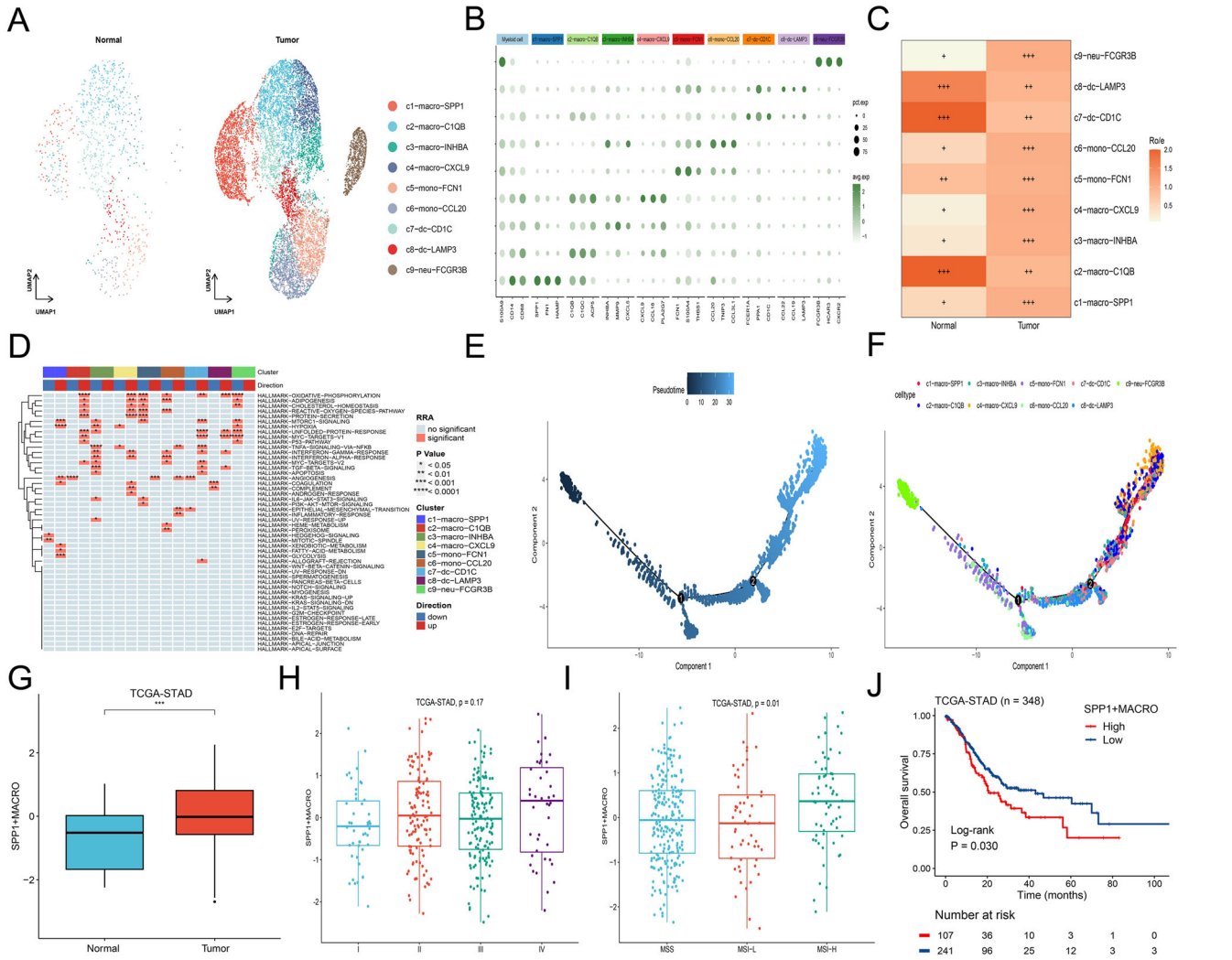

Fig. 3 | Characterization of myeloid cells in GC patients. A UMAP plot showing the composition of myeloid cells colored by cluster. **B** Dot plot showing the top three differentially expressed genes of 9 myeloid cell clusters. **C** Tissue preference of each myeloid cell cluster estimated by Ro/e score. +++, Ro/e > 1; ++, 0.8 < Ro/e ≤ 1; +, 0.2 ≤ Ro/e ≤ 0.8; ±, 0 < Ro/e < 0.2; −, Ro/e = 0. **D** GSVA plot showing the terms of the hallmark gene set enrichment pathway for each myeloid cell cluster. **E** The pseudotime of the developmental trajectory inferred by Monocle 2. **F** Myeloid cell transition along the pseudotime trajectory. **G** Quantification of SPP1+ macrophage in TCGA-STAD dataset. **H** Association between SPP1+ macrophage and TNM stage. **I** Association between SPP1+ macrophage and microsatellite status. **J** K-M curves of OS in TCGA-STAD dataset grouped by SPP1+ macrophage.

Analysis of GREM1+ fibroblasts and SPP1+ macrophages in pan-cancer cohort

To further explore whether GREM1+ fibroblasts and SPP1+ macrophages exist and exert functions in other solid tumors as well, we collected 129 scRNA-seq samples from 10 common solid tumors for pan-cancer analysis. We identified 42, 248 fibroblasts and obtained 13 fibroblast subclusters, named c1-APOD ($n = 13128$), c2-PLA2G2A ($n = 6528$), c3-CTHRC1 ($n = 5364$), c4-IGFBP5 ($n = 4533$), c5-MYH11 ($n = 4416$), c6-APOE ($n = 3849$), c7-RGS5 ($n = 2058$), c8-SERPINE2 ($n = 621$), c9-SRGN ($n = 546$), c10-GREM1 ($n = 448$), c11-TOP2A ($n = 442$), c12-IL33 ($n = 257$) and c13-MSLN ($n = 58$), respectively (Fig. 9A). Among them, c10-fibro-GREM1 highly expressed GREM1+ fibroblasts marker genes, and accounted for a significantly higher proportion in tumor tissues (Fig. 9B, C). Similarly, we identified 29, 527 macrophages in the pan-cancer cohort, and further clustered into 10 subclusters, named c1-APOE ($n = 6101$), c2-CCL4 ($n = 5053$), c3-FOLR3 ($n = 3954$), c4-SPP1 ($n = 3483$), c5-FABP4 ($n = 2899$), c6-RGS1 ($n = 2879$), c7-S100A8 ($n = 1761$), c8-CXCL9 ($n = 1269$), c9-SLC40A1 ($n = 1107$) and c10-FTL ($n = 1021$), respectively (Fig. 9D). c4-macro-SPP1 highly expressed SPP1+ macrophages marker genes, and were significantly enriched in tumor tissues (Fig. 9E, F). In the 15 solid tumor types of TCGA, GREM1+ fibroblasts were significantly upregulated in BRCA, CHOL, COAD, ESCA, HNSC, KIRC, LUAD, LUSC, and READ, while SPP1+ macrophages were significantly upregulated in BRCA, CHOL, ESCA, HNSC, KIRC, LUAD, and THCA (Fig. S7). Scatter plots showed that GREM1+ fibroblasts and SPP1+ macrophages were positively correlated in all types of solid tumors (Fig. S8). Kaplan-Meier analysis indicated that patients with high expression of GREM1+ fibroblasts and SPP1+ macrophages were associated with poor survival across a pan-cancer cohort of 6, 503 TCGA tumor samples from 15 cancer types (Fig. 9G–I).

Discussion

Gastric cancer is among the most lethal malignancies and poses a serious threat to human health[21]. The molecular characteristics of GC differ greatly among different patients, which may be one of the biggest factors leading to poor treatment results[22,23]. Precision medicine research based on individual genetic characteristics and molecular typing can help us to deeply analyze the heterogeneity of GC and develop new targeted drugs and treatment strategies[24–26]. Therefore, there is an urgent need to apply scRNA-seq and ST technology to the

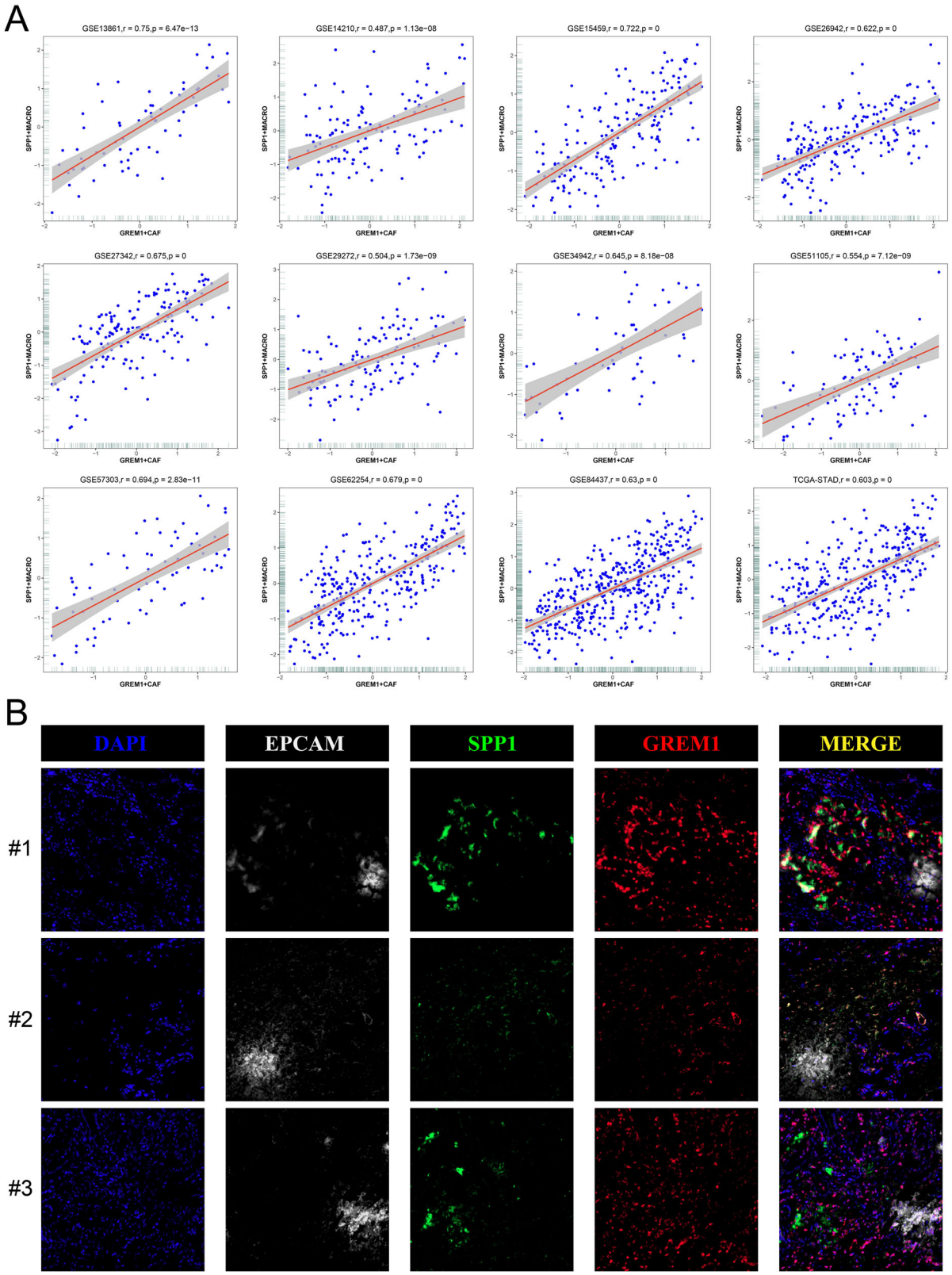

Fig. 4 | Interactions between GREM1+ fibroblasts and SPP1+ macrophages. **A** Scatter plots showing the correlation between the score of GREM1+ fibroblast and SPP1+ macrophage across 12 independent GC datasets. **B** Representative immunofluorescent labeling of human GC tissue (20x). DAPI (blue), EPCAM (gray), SPP1 (green), GREM1 (red), MERGE (yellow) in patient #1, #2, and #3.

analysis of GC. Based on the above background, we performed this multi-omics study to analyze the heterogeneity of GC microenvironment and explore the interactions between fibroblasts and macrophages.

Fibroblasts are the most common mesenchymal cells in the TME, and are closely related to tumor immune escape, progression, and treatment resistance[27,28]. Luo et al. identified 8 fibroblast subpopulations in the pan-cancer scRNA-seq cohort and found that CAF highly expressed genes

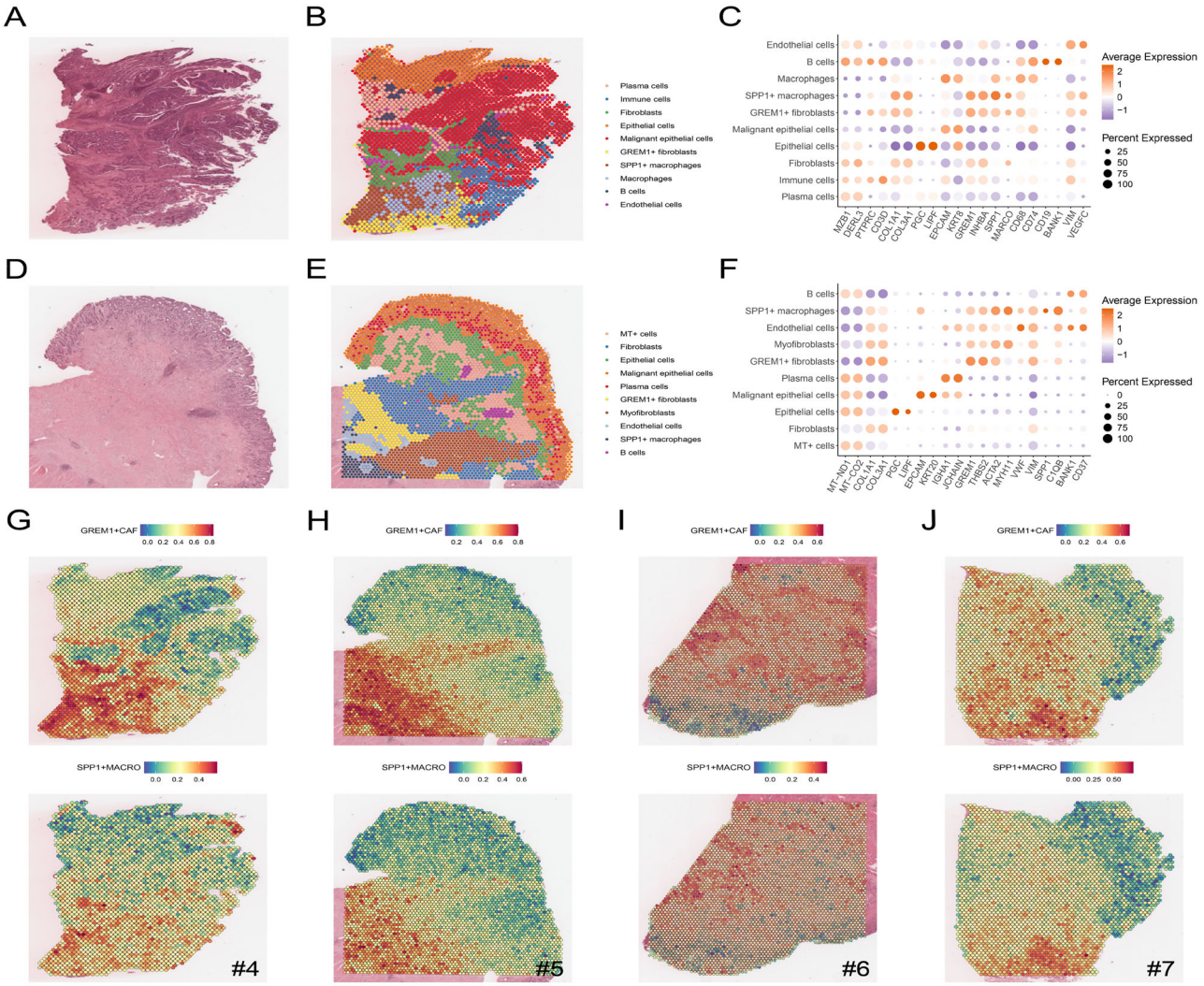

Fig. 5 | Co-localization of GREM1+ fibroblasts and SPP1+ macrophages revealed by spatial transcriptomics. A Hematoxylin and eosin (H&E) staining of tissue sections of ST spots in GC patient #4. **B** Unbiased clustering of ST spots and define cell types of each cluster. **C** Dot plots showing the known markers in indicated cell clusters. **D** H&E staining of tissue sections of ST spots in GC patient #5. **E** Unbiased clustering of ST spots and define cell types of each cluster. **F** Dot plots showing the known markers in indicated cell clusters. **G**–**J** Spatial feature plots of signature score of GREM1+ fibroblast and SPP1+ macrophage in patient #4, #5, #6, and #7.

related to collagen activation and matrix metalloproteinases[29]. Sun et al. found that Fib_1 highly expressed matrix metalloproteinases such as MMP3 and MMP11, which could regulate the structure of extracellular matrix[30]. In addition, the Fib_1 showed positive feedback up-regulation of the TWIST1/PRRX1/TNC pathway, promoting the expansion and activation of CAF. The analysis presented above further demonstrated that fibroblasts displayed a high degree of heterogeneity in the TME. In this study, we systemically deciphered the features of fibroblasts and demonstrated their functional heterogeneity. Consistent with previous single-cell fibroblast studies, our study confirmed the presence of known fibroblast subtypes, such as POSTN+ myofibroblasts, HILPDA+ vascular-like fibroblasts, and C7+ inflammatory fibroblasts[31]. Importantly, we identified GREM1+ fibroblasts, which were significantly enriched in GC tissues and had the highest scores for EMT, angiogenesis, and M2 macrophage polarization. Patients with high expression of GREM1+ fibroblasts were correlated with poor TNM stage and prognosis, indicating that GREM1+ fibroblasts could promote GC progression.

The functions of TAMs are diverse and can be affected by different stimulation and regulatory mechanisms[32]. Understanding and intervening the function of TAMs is helpful to develop new anti-tumor treatment strategies and ultimately improve therapeutic efficacy. Cheng et al. analyzed 380 samples of scRNA-seq and found 6 TAM subpopulations: INHBA + TAM, C1QC + TAM, ISG15 + TAM, LNRP3 + TAM, LYVE1 + TAM, and SPP1 + TAM[33]. Macrophage subpopulations from different tumor types showed high heterogeneity, which may be related to the different effects of local TME. Li et al. found that M08 subpopulations highly expressed INHBA, PTGS2, and a variety of pro-inflammatory cytokines and chemokines, while M09 and M10 highly expressed genes related to antigen presentation[34]. In our study, SPP1+ macrophages were significantly enriched in GC tissues and had the highest M2 macrophage polarization scores. Furthermore, patients with high expression of SPP1+ fibroblasts were associated with poor TNM stage and survival.

Accumulating evidence indicated that there is a close association between macrophages and fibroblasts[35–37]. Su et al. found that FAP+ fibroblasts and SPP1+ macrophages can interact through signaling pathways such as VEGF, ECM, and hypoxia, jointly forming a unique TME that promotes the progression of patients with pMMR[38]. Li et al. found that THBS2+ CAFs and SPP1+ TAMs could modulate the immunotherapeutic effect of GC patients through the C3-C3AR1 axis[39]. In this study, spatial transcriptomic analysis revealed that GREM1+ fibroblasts and SPP1+ macrophages were located in adjacent regions. GREM1+ fibroblasts can

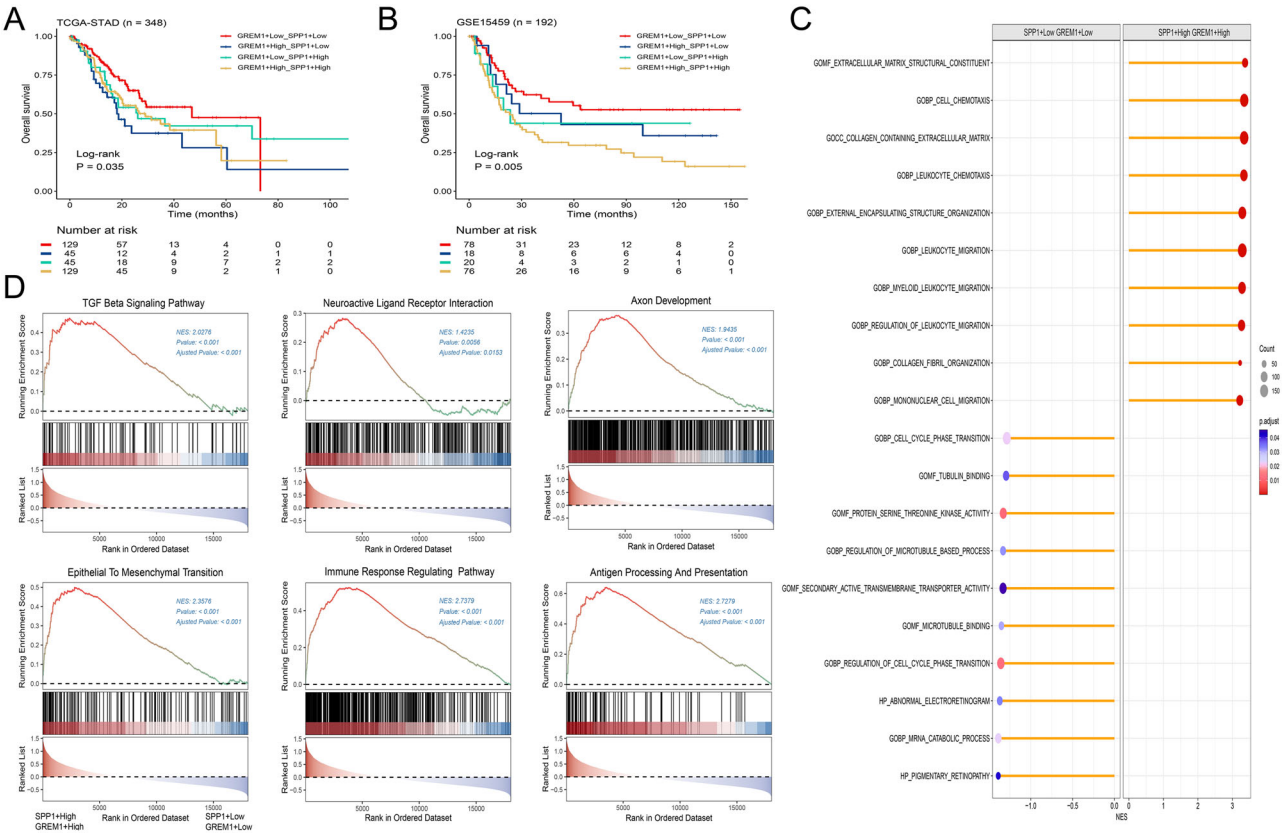

Fig. 6 | High expression of GREM1+ fibroblasts and SPP1+ macrophages was associated with worse prognosis and cancer-related pathways. A, **B** K-M curves of OS in TCGA-STAD and GSE15459 datasets according to the expression of GREM1+ fibroblast and SPP1+ macrophage. **C** GO analysis of pathways between GREM1+ fibroblast^{high}/SPP1+ macrophage^{high} and GREM1+ fibroblast^{low}/SPP1+ macrophage^{low} groups. **D** GSEA analysis of pathways between GREM1+ fibroblast^{high}/SPP1+ macrophage^{high} and GREM1+ fibroblast^{low}/SPP1+ macrophage^{low} groups.

directly contact with SPP1+ macrophages through COLLAGEN signaling pathway, while SPP1+ macrophages can act on GREM1+ fibroblasts through SPP1 signaling pathway. These results unravel the complex interactions between GREM1+ fibroblasts and SPP1+ macrophages, which may serve as a potential therapeutic target for future GC treatment.

GC is a highly heterogeneous disease, making treatment responses difficult to predict. Therefore, a better understanding of the molecular mechanism of GC is crucial for diagnosis, treatment, and prognosis[40]. In this study, patients were grouped based on the infiltration levels of GREM1+ fibroblasts and SPP1+ macrophages, and the proportion of diffuse subtype in the high group was significantly higher than that in the low group. Patients with both high GREM1+ fibroblasts and SPP1+ macrophages exhibited significantly shorter OS and showed enrichment of tumor-associated pathways such as TGF-β, epithelium-to-mesenchymal transformation, and antigen processing and presentation. Additionally, Kaplan-Meier analysis demonstrated that patients in the high group had worse survival outcomes after receiving immunotherapy. These results enriched our understanding of the mechanisms of GC and may provide a new therapeutic target for the treatment of GC.

Given the strong association between these two cell types in GC patients, we wondered whether other pan-cancer types present such pattern at some appreciable level. Qi et al. found that the synergistic effect between FAP+ fibroblasts and SPP1+ macrophages can reshape the extracellular matrix and ultimately form a microenvironment that prevents lymphocytes from infiltrating into the tumor core and reduces the efficacy of immunotherapy[41]. Li et al. demonstrated that SPP1+ APOE+ TAMs and CTHRC1+ GREM1+ CAFs may act synergistically to promote an immune-suppressive TME through active extracellular matrix deposition and epithelial-mesenchymal transition, resulting in poor prognosis for patients with pancreatic ductal adenocarcinoma[42]. There have also been a number of studies investigating the role of fibroblasts and macrophages in other solid tumors[43,44]. In this study, we collected 129 scRNA-seq samples from 10 common solid tumors. GREM1+ fibroblasts and SPP1+ macrophages accounted for a significantly higher proportion in tumor tissues. Moreover, Kaplan-Meier analysis indicated that patients with high expression of GREM1+ fibroblasts and SPP1+ macrophages were correlated with poor survival across a pan-cancer cohort. These results suggest that the interactions between GREM1+ fibroblasts and SPP1+ macrophages not only exist in gastric cancer but can also synergistically promote tumor progression in various solid tumors. We believe that in-depth analysis of these data will provide new insights for studying the role of fibroblast-macrophage in the tumor microenvironment.

There were also some limitations to this study. First, because of the relatively small number of patients, it was difficult to value the relationship between specific cell types and patient prognosis using the scRNA-seq data. Second, factors such as sampling strategy, variability in the distribution of cells, tissue heterogeneity, and histological processing might also affect the results. Third, patients included in the present analysis received a variety of treatment regimens, which may have affected patient outcomes. Future experimental verification is needed to elucidate the role of GREM1+ fibroblasts and SPP1+ macrophages in the tumor microenvironment.

In this study, we combined bulk RNA-seq, scRNA-seq, and spatial transcriptomics to explore the detailed landscape of GC microenvironment. Both GREM1+ fibroblasts and SPP1+ macrophages were significantly enriched in GC tissues and were associated with poor patient prognosis. We then demonstrated the complex interactions between GREM1+ fibroblasts and SPP1+ macrophages, which may serve as a potential therapeutic target for future treatment of GC.

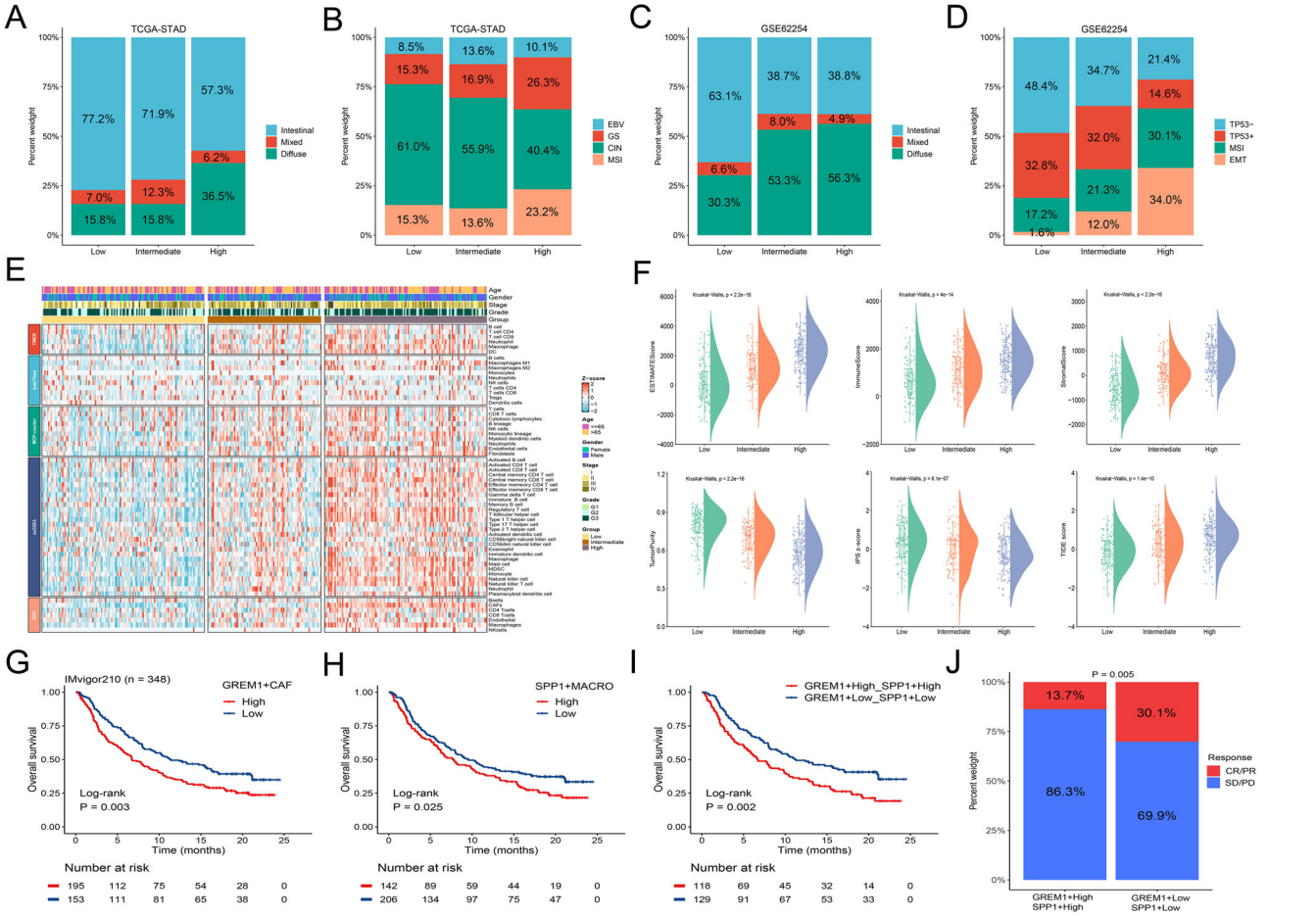

Fig. 7 | The molecular subtypes and immune landscapes of GC patients affected by GREM1+ fibroblasts and SPP1+ macrophages. The association between GREM1+ fibroblast/SPP1+ macrophage type and Lauren (**A**) and TCGA (**B**) type in TCGA-STAD dataset. The association between GREM1+ fibroblast/SPP1+ macrophage type and Lauren (**C**) and ACRG (**D**) type in GSE62254 dataset. **E** Correlation between GREM1+ fibroblast/SPP1+ macrophage type and tumor-infiltrating immune cells. **F** Box plots displaying the ESTIMATE score, immune score, stromal score, tumor purity, IPS z-score, and TIDE score between GREM1+ fibroblast/SPP1+ macrophage subtypes. **G–I** K-M curves of OS in IMvigor210 dataset grouped by GREM1+ fibroblast and SPP1+ macrophage. **J** Distribution of the immunotherapy responses according to GREM1+ fibroblast/SPP1+ macrophage type. CR complete response, PR partial response, SD stable disease, PD progressive disease.

Methods

Data sources

In this study, the training cohort consisted of four public scRNA-seq datasets, and the validation cohort was obtained from 10 GC patients who underwent radical tumor resection with histologically confirmed diagnosis at the Chinese PLA General Hospital between October 2023 and December 2023 (Table S1 and Table S2). For bulk sequencing, messenger RNA (mRNA) expression profiles were obtained from the TCGA and GEO databases. A total of 12 cohorts including GSE13861, GSE14210, GSE15459, GSE26942, GSE27342, GSE29272, GSE34942, GSE51105, GSE57303, GSE62254, GSE84437 and TCGA-STAD were enrolled. This study was approved by the Ethical Committee of Chinese PLA General Hospital (Approval number: S2022-313-02), and was in accordance with the Declaration of Helsinki. Written informed consent was obtained from all enrolled patients.

In the pan-cancer analysis, we collected 129 scRNA-seq samples from 10 common solid tumors, including 72 tumor tissues and 57 adjacent normal tissues (Table S3). Subsequently, the gene expression matrix and survival data of 15 solid tumors in the TCGA database were downloaded using the "easyTCGA" package, which was used to analyze the correlation between GREM1+ fibroblasts and SPP1+ macrophages and their influence on patient prognosis.

Single-cell RNA sequencing analysis

Raw scRNA-seq data were processed with Cell Ranger (version 7.1.0) to obtain the unique molecular identifiers (UMI) and generate feature-barcode expression matrices. After quality controls, reads were aligned on the reference genome GRCh38 using default parameters. The "Seurat" R package was used to process the scRNA-seq data[45]. Cells with gene expression less than 500 or greater than 6000 or mitochondria genes greater than 15% were excluded. The "decontx" R package was used to eliminate potential RNA contamination[46]. Batch effects were then corrected with the "harmony" package[47]. The UMAP analyses were used for cluster visualization, and annotated 9 main cell types using typical marker genes.

Tissue distribution of clusters

We calculated the ratio of observed over expected cell numbers (Ro/e) to quantify the tissue preference of each cluster[48]. The expected cell numbers for each cell cluster and tissue combination were obtained by chi-square test. Clusters were considered to be enriched in a specific tissue if Ro/e > 1.

Differential gene expression analysis

Differential gene expression analysis can explore differences between different cell types or states, which can help better understand the tumor microenvironment. The "FindAllMarkers" function and Wilcoxon

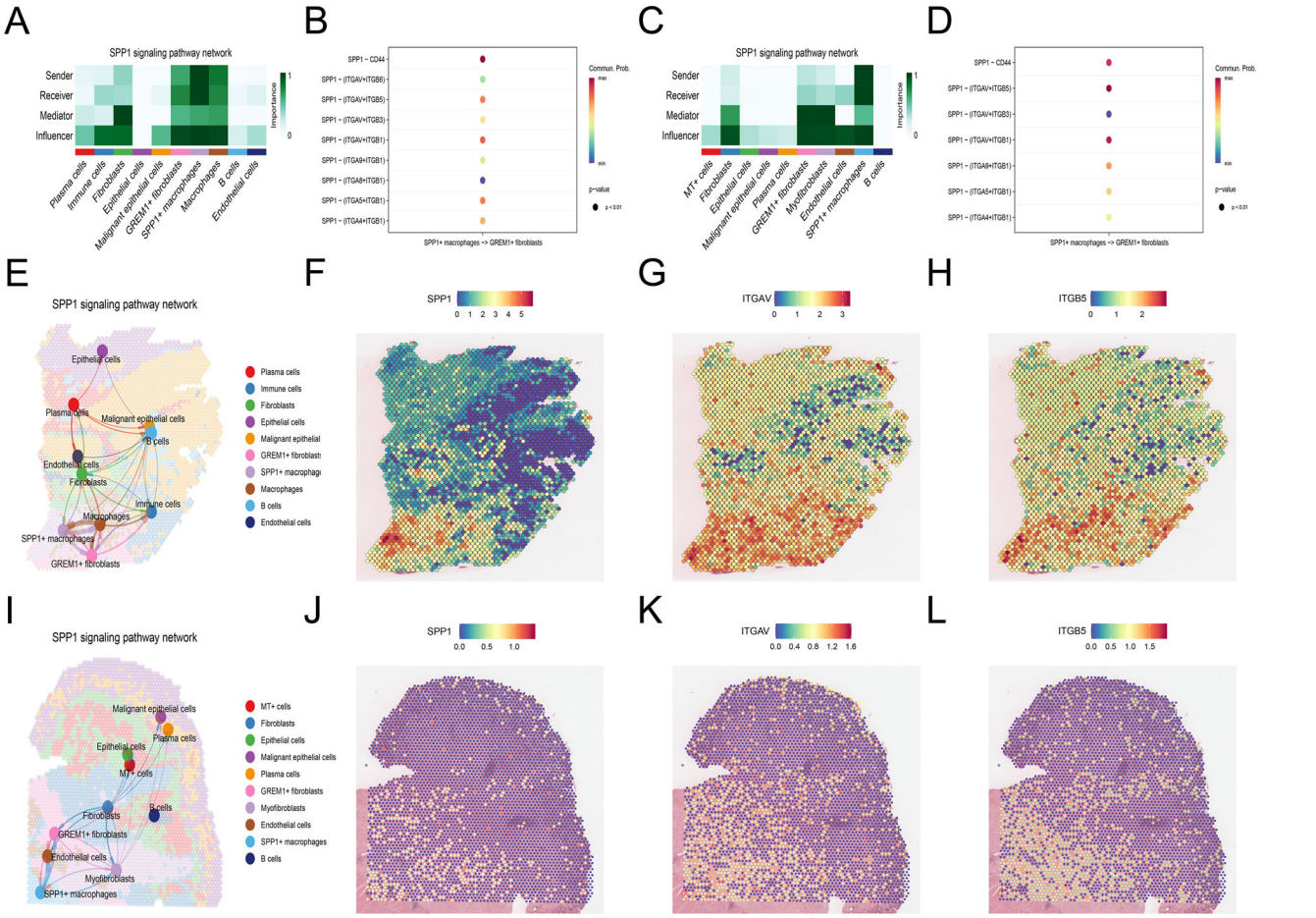

Fig. 8 | The interaction network between GREM1+ fibroblasts and SPP1+ macrophages revealed by spatial transcriptomics. A Heatmap showing the SPP1 signaling pathway in patient #4. **B** Dot plot showing the SPP1 signaling pathway in patient #4. **C** Heatmap showing the SPP1 signaling pathway in patient #5. **D** Dot plot showing the SPP1 signaling pathway in patient #5. **E** The interaction network of the SPP1 signaling pathway in patient #4. **F**–**H** Spatial images localize the expression of the SPP1 signaling pathway in patient #4. **I** The interaction network of the SPP1 signaling pathway in patient #5. **J**–**L** Spatial images localize the expression of the SPP1 signaling pathway in patient #5.

rank sum test were used to analyze differentially expressed genes between different cell subpopulations. Genes were considered differentially expressed if log2FC was more than 1 and the FDR adjusted *p*-value was less than 0.05.

Pathway enrichment analysis

Pathway enrichment analysis was performed with the "irGSEA" package implemented under the R software environment[49]. Based on scRNA-seq data and gene set database, different cell subpopulations were enriched by "AUCell", "UCell", "singscore", and "ssgsea" functions, and the rank aggregation algorithm was used for comprehensive evaluation. Furthermore, we used the "AddModuleScore" function to score the cell subpopulations based on different functional gene sets, and analyzed the specific functions of the cell subpopulations. The functional gene sets presented in this study were derived from the summaries of previous literature[10,50].

Pseudotime trajectory analysis

The "Monocle" package is a pseudotime based analysis algorithm, which can infer cell development tracks from dynamic changes in the scRNA-seq data[51]. In this study, we used the "newCellDataSet" function to create pseudo-timing analysis objects and used the "differentialGeneTest" function to select 2000 genes that were most relevant to the pseudo-timing model. Finally, the "DDRTree" algorithm was used to conduct a dimension reduction analysis of cell features in high-dimensional space, and the "plot_cell_trajectory" function was used to visualize the trajectory.

Intercellular communication analysis amongst GC clusters

The "CellChat" package can analyze cell-cell interactions based on the expression levels of ligand-receptor pairs[52]. "identifyOverExpressedGenes", "identifyOverExpressedInteractions", "computeCommunProb", and "aggregateNet" functions were successively applied to deal with scRNA-seq and spatial transcriptomics data. Finally, the results were visualized by "netVisual_circle", "netVisual_heatmap", "netVisual_bubble", and "netVisual_aggregate" functions.

Immune landscape and immunotherapy efficacy

The "ssGSEA" function was applied to infer the infiltration levels of 28 immune cells within each sample[53]. To ensure stability, four other algorithms, including TIMER, quanTIseq, MCP-counter, and EPIC, were also carried out to examine the consequence of immune cell infiltration[54–57]. The TIDE algorithm was then employed to predict the likelihood of immunotherapy response of GC patients[58]. In addition, we used the IMvigor210 cohort to analyze the immunotherapy efficacy based on the infiltration levels of GREM1+ fibroblasts and SPP1+ macrophages.

Survival analysis

To explore the role of GREM1+ fibroblasts and SPP1+ macrophages in predicting prognosis, we assessed the infiltration level of the two cell types using the "ssGSEA" function (the top 30 specifically expressed genes in the scRNA-seq data, Table S4). Subsequently, the prognostic significance was assessed by Kaplan-Meier analysis.

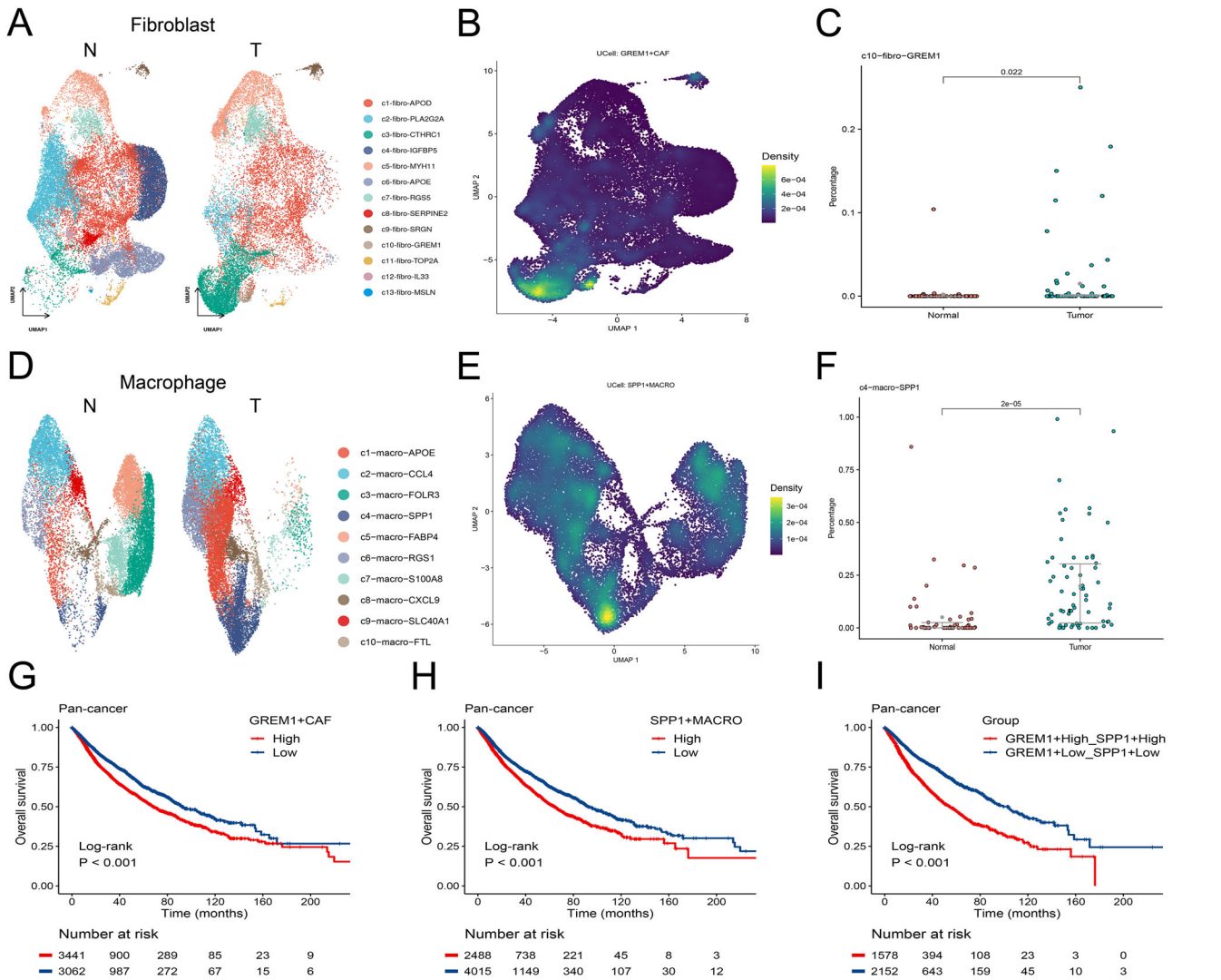

Fig. 9 | Characterization of GREM1+ fibroblasts and SPP1+ macrophages in pan-cancer cohort. A UMAP showing the composition of fibroblasts colored by cluster. **B** Signature score of GREM1+ fibroblast. **C** Proportion of GREM1+ fibroblast in different tissues. **D** UMAP showing the composition of macrophages colored by cluster. **E** Signature score of SPP1+ macrophage. **F** Proportion of SPP1+ macrophage in different tissues. **G–I** K-M curves of OS grouped by GREM1+ fibroblast and SPP1+ macrophage.

Spatial transcriptomics data analysis

Spatial Transcriptomics slides can simultaneously capture approximately 3000-5000 markers with two identical capture areas and obtain spatial location and sequencing results. The "Load10X_Spatial" function was used to read the spatial transcriptome data, and exclude markers with the total number of genes less than 500 or the proportion of mitochondrial genes more than 30%. Subsequently, the "SCTransform" function was used for standardization, screening of highly variable genes and normalization. The "RunPCA" function was then used to identify the main sources of change in the spatial transcriptome data, and the first 30 PCs were selected for clustering, with a unified resolution of 1.2. "FindNeighbors" and "FindClusters" were used for unsupervised cluster analysis, and "RunUMAP" was applied to generate a coordinate matrix that visualized the location of individual marker points onto a two-dimensional plane.

Multiplex immunohistochemistry staining

Multiplex immunohistochemistry (mIHC) is an assay to visualize multiple antigens simultaneously on the tissue. The GC samples used for mIHC analysis were obtained from surgical specimens previously who signed informed consent forms. Primary antibodies included EPCAM mouse anti-human antibody (cat. No. 14-9326-82, invitrogen, 1:200), SPP1 rabbit anti-human antibody (Cat. No. MA5-17180, invitrogen, 1:200), and GREM1 rabbit anti-human antibodies (cat. No. PA1-41012, invitrogen, 1:150). Slides were dewaxed and hydrated, and heat-induced antigen retrieval was then performed. A TSA Fluorescence Kit was used to stain the primary antibodies, and all the experimental procedures were performed according to the manufacturer's instructions. After staining, fluorescent staining was observed and photographed under fluorescence microscope.

Statistical analysis

Pearson correlation analysis was used to assess the strength and direction of the linear relationship between two variables. The Mann-Whitney U test was used to compare the proportion of different cell subpopulations, and the comparative analysis among multiple groups was performed using Kruskal–Wallis test. All statistical analyses in this study were performed using R 4.1.0 software. $P < 0.05$ was considered statistically significant.

Data availability

The raw data can be found in the TCGA (https://portal.gdc.cancer.gov/), UCSC Xena (https://xenabrowser.net/), and GEO (https://www.ncbi.

nlm.nih.gov/geo/) database. The raw data that support the findings of this study are available from the corresponding author upon reasonable request.

Code availability

All codes used in this analysis were run in R v4.1.0 and are available from the corresponding authors upon reasonable request.

Received: 25 December 2024; Accepted: 27 May 2025;
Published online: 05 June 2025

References

1. Smyth, E. C., Nilsson, M., Grabsch, H. I., van Grieken, N. C. & Lordick, F. Gastric cancer. *Lancet* **396**, 635–648 (2020).
2. Waldum, H. & Fossmark, R. Gastritis, gastric polyps and gastric cancer. *Int. J. Mol. Sci.* **22**, 6548 (2021).
3. Machlowska, J., Baj, J., Sitarz, M., Maciejewski, R. & Sitarz, R. Gastric cancer: epidemiology, risk factors, classification, genomic characteristics and treatment strategies. *Int. J. Mol. Sci.* **21**, 4012 (2020).
4. Li, K., Zhang, A., Li, X., Zhang, H. & Zhao, L. Advances in clinical immunotherapy for gastric cancer. *Biochim. Biophys. Acta Rev. Cancer* **1876**, 188615 (2021).
5. Patel, T. H. & Cecchini, M. Targeted therapies in advanced gastric cancer. *Curr. Treat. Options Oncol.* **21**, 70 (2020).
6. Lordick, F. et al. Gastric cancer: ESMO clinical practice guideline for diagnosis, treatment and follow-up. *Ann. Oncol.* **33**, 1005–1020 (2022).
7. DeBerardinis, R. J. Tumor microenvironment, metabolism, and immunotherapy. *N. Engl. J. Med.* **382**, 869–871 (2020).
8. Jiang, X. et al. The role of microenvironment in tumor angiogenesis. *J. Exp. Clin. Cancer Res.* **39**, 204 (2020).
9. Lavie, D., Ben-Shmuel, A., Erez, N. & Scherz-Shouval, R. Cancer-associated fibroblasts in the single-cell era. *Nat. Cancer* **3**, 793–807 (2022).
10. Ma, C. et al. Pan-cancer spatially resolved single-cell analysis reveals the crosstalk between cancer-associated fibroblasts and tumor microenvironment. *Mol. Cancer* **22**, 170 (2023).
11. Zhang, Q. & Sioud, M. Tumor-associated macrophage subsets: shaping polarization and targeting. *Int. J. Mol. Sci.* **24**, 7493 (2023).
12. Gao, J., Liang, Y. & Wang, L. Shaping polarization of tumor-associated macrophages in cancer immunotherapy. *Front. Immunol.* **13**, 888713 (2022).
13. Han, S. et al. d-lactate modulates M2 tumor-associated macrophages and remodels immunosuppressive tumor microenvironment for hepatocellular carcinoma. *Sci. Adv.* **9**, eadg2697 (2023).
14. Gunaydin, G. CAFs interacting With TAMs in tumor microenvironment to enhance tumorigenesis and immune evasion. *Front. Oncol.* **11**, 668349 (2021).
15. Herrera, M. et al. Cancer-associated fibroblast and M2 macrophage markers together predict outcome in colorectal cancer patients. *Cancer Sci.* **104**, 437–444 (2013).
16. Tan, B. et al. Inhibition of Rspo-Lgr4 facilitates checkpoint blockade therapy by switching macrophage polarization. *Cancer Res.* **78**, 4929–4942 (2018).
17. Comito, G. et al. Cancer-associated fibroblasts and M2-polarized macrophages synergize during prostate carcinoma progression. *Oncogene* **33**, 2423–2431 (2014).
18. Zhang, Q. et al. Macrophages activate mesenchymal stem cells to acquire cancer-associated fibroblast-like features resulting in gastric epithelial cell lesions and malignant transformation in vitro. *Oncol. Lett.* **17**, 747–756 (2019).
19. Gao, Z., Houthuijzen, J. M., Ten Dijke, P. & Brazil, D. P. GREM1 signaling in cancer: tumor promotor and suppressor?. *J. Cell Commun. Signal.* **17**, 1517–1526 (2023).
20. Yang, X. et al. SPP1 promotes the polarization of M2 macrophages through the Jak2/Stat3 signaling pathway and accelerates the progression of idiopathic pulmonary fibrosis. *Int. J. Mol. Med.* **54**, 89 (2024).
21. López, M. J. et al. Characteristics of gastric cancer around the world. *Crit. Rev. Oncol. Hematol.* **181**, 103841 (2023).
22. Jiang, H. et al. Revealing the transcriptional heterogeneity of organ-specific metastasis in human gastric cancer using single-cell RNA Sequencing. *Clin. Transl. Med.* **12**, e730 (2022).
23. Qing, X. et al. Molecular characteristics, clinical significance, and cancer immune interactions of angiogenesis-associated genes in gastric cancer. *Front Immunol.* **13**, 843077 (2022).
24. Xu, H., Jiao, D., Liu, A. & Wu, K. Tumor organoids: applications in cancer modeling and potentials in precision medicine. *J. Hematol. Oncol.* **15**, 58 (2022).
25. He, X., Liu, X., Zuo, F., Shi, H. & Jing, J. Artificial intelligence-based multi-omics analysis fuels cancer precision medicine. *Semin. Cancer Biol.* **88**, 187–200 (2023).
26. Yuan, J., Li, X. & Yu, S. Cancer organoid co-culture model system: Novel approach to guide precision medicine. *Front. Immunol.* **13**, 1061388 (2022).
27. Zhang, H. et al. Define cancer-associated fibroblasts (CAFs) in the tumor microenvironment: new opportunities in cancer immunotherapy and advances in clinical trials. *Mol. Cancer* **22**, 159 (2023).
28. Chen, Y., McAndrews, K. M. & Kalluri, R. Clinical and therapeutic relevance of cancer-associated fibroblasts. *Nat. Rev. Clin. Oncol.* **18**, 792–804 (2021).
29. Luo, H. et al. Pan-cancer single-cell analysis reveals the heterogeneity and plasticity of cancer-associated fibroblasts in the tumor microenvironment. *Nat. Commun.* **13**, 6619 (2022).
30. Sun, K. et al. scRNA-seq of gastric tumor shows complex intercellular interaction with an alternative T cell exhaustion trajectory. *Nat. Commun.* **13**, 4943 (2022).
31. Liu, K. et al. Fibroblast atlas: shared and specific cell types across tissues. *Sci. Adv.* **11**, eado0173 (2025).
32. Pan, Y., Yu, Y., Wang, X. & Zhang, T. Tumor-associated macrophages in tumor immunity. *Front. Immunol.* **11**, 583084 (2020).
33. Cheng, S. et al. A pan-cancer single-cell transcriptional atlas of tumor infiltrating myeloid cells. *Cell* **184**, 792–809.e723 (2021).
34. Li, Y. et al. Single-cell landscape reveals active cell subtypes and their interaction in the tumor microenvironment of gastric cancer. *Theranostics* **12**, 3818–3833 (2022).
35. Mao, X. et al. Crosstalk between cancer-associated fibroblasts and immune cells in the tumor microenvironment: new findings and future perspectives. *Mol. Cancer* **20**, 131 (2021).
36. Sathe, A. et al. Colorectal cancer metastases in the liver establish immunosuppressive spatial networking between tumor-associated SPP1+ macrophages and fibroblasts. *Clin. Cancer Res.* **29**, 244–260 (2023).
37. Hoeft, K. et al. Platelet-instructed SPP1(+) macrophages drive myofibroblast activation in fibrosis in a CXCL4-dependent manner. *Cell Rep.* **42**, 112131 (2023).
38. Su, Z. et al. SPP1+ macrophages and FAP+ fibroblasts promote the progression of pMMR gastric cancer. *Sci. Rep.* **14**, 26221 (2024).
39. Li, Y. et al. CAF-macrophage crosstalk in tumour microenvironments governs the response to immune checkpoint blockade in gastric cancer peritoneal metastases. *Gut* **74**, 350–363 (2025).
40. Bagaev, A. et al. Conserved pan-cancer microenvironment subtypes predict response to immunotherapy. *Cancer Cell* **39**, 845–865.e847 (2021).
41. Qi, J. et al. Single-cell and spatial analysis reveal interaction of FAP(+) fibroblasts and SPP1(+) macrophages in colorectal cancer. *Nat. Commun.* **13**, 1742 (2022).

42. Li, E., Cheung, H. C. Z. & Ma, S. CTHRC1(+) fibroblasts and SPP1(+) macrophages synergistically contribute to pro-tumorigenic tumor microenvironment in pancreatic ductal adenocarcinoma. *Sci. Rep.* **14**, 17412 (2024).
43. Chen, C. et al. Single-cell and spatial transcriptomics reveal POSTN(+) cancer-associated fibroblasts correlated with immune suppression and tumour progression in non-small cell lung cancer. *Clin. Transl. Med.* **13**, e1515 (2023).
44. Gao, Y. et al. Cross-tissue human fibroblast atlas reveals myofibroblast subtypes with distinct roles in immune modulation. *Cancer Cell* **42**, 1764–1783.e1710 (2024).
45. Stuart, T. et al. Comprehensive integration of single-cell data. *Cell* **177**, 1888–1902.e1821 (2019).
46. Yang, S. et al. Decontamination of ambient RNA in single-cell RNA-seq with DecontX. *Genome Biol.* **21**, 57 (2020).
47. Korsunsky, I. et al. Fast, sensitive and accurate integration of single-cell data with Harmony. *Nat. Methods* **16**, 1289–1296 (2019).
48. Zhang, L. et al. Lineage tracking reveals dynamic relationships of T cells in colorectal cancer. *Nature* **564**, 268–272 (2018).
49. Fan, C. et al. irGSEA: the integration of single-cell rank-based gene set enrichment analysis. *Brief. Bioinform.* **25**, bbae243 (2024).
50. Azizi, E. et al. Single-cell map of diverse immune phenotypes in the breast tumor microenvironment. *Cell* **174**, 1293–1308.e1236 (2018).
51. Qiu, X. et al. Reversed graph embedding resolves complex single-cell trajectories. *Nat. Methods* **14**, 979–982 (2017).
52. Jin, S. et al. Inference and analysis of cell-cell communication using CellChat. *Nat. Commun.* **12**, 1088 (2021).
53. Hänzelmann, S., Castelo, R. & Guinney, J. GSVA: gene set variation analysis for microarray and RNA-seq data. *BMC Bioinforma.* **14**, 7 (2013).
54. Li, T. et al. TIMER: a web server for comprehensive analysis of tumor-infiltrating immune cells. *Cancer Res.* **77**, e108–e110 (2017).
55. Plattner, C., Finotello, F. & Rieder, D. Deconvoluting tumor-infiltrating immune cells from RNA-seq data using quanTIseq. *Methods Enzymol.* **636**, 261–285 (2020).
56. Becht, E. et al. Estimating the population abundance of tissue-infiltrating immune and stromal cell populations using gene expression. *Genome Biol.* **17**, 218 (2016).
57. Racle, J., de Jonge, K., Baumgaertner, P., Speiser, D. E. & Gfeller, D. Simultaneous enumeration of cancer and immune cell types from bulk tumor gene expression data. *Elife* **6**, e26476 (2017).
58. Jiang, P. et al. Signatures of T cell dysfunction and exclusion predict cancer immunotherapy response. *Nat. Med.* **24**, 1550–1558 (2018).

Acknowledgements

We thank Beijing DCTY Biotech Co., Ltd. for support of this research.

Author contributions

L.P.Q., S.C.J., and J.M.X. designed this study, L.P.Q. analyzed and interpreted the data, L.P.Q., Y.F., and X.Z. wrote this manuscript. S.Y., Y.X.G., Z.S.Z., and J.M.X. edited and revised the manuscript. All authors have approved the final version of the manuscript.

Competing interests

The authors declare no competing interests.

Additional information

Supplementary information The online version contains supplementary material available at https://doi.org/10.1038/s41698-025-00967-w.

Correspondence and requests for materials should be addressed to Shunchang Jiao or Jianming Xu.